C'mon Part, do the Local Motion!

Dan S. Reznik and John F. Canny
{dreznik,jfc}@cs.berkeley.edu
EECS Department, UC–Berkeley

Abstract – *We describe a new control method for vibrations-based planar manipulation. We've developed a device – the Universal Planar Manipulator (UPM) – based on a single, horizontally-vibrating plate. Though minimalist in construction (one moving part), the UPM can manipulate several parts on its surface in parallel, simply using friction. Previously, we've shown that a sequence of rigid plate rotations can be computed which produces pre-specified part displacements. Here we present a new method based on a special motion primitive – the "jet" – which displaces a chosen part in a desired direction while keeping all others still. A jet allows one to say: "c'mon part, do a local motion". Parallel manipulation then reduces to a round-robin application of jets. This technique is both faster and more robust than the old rotations-based method. Experiments on parallel trajectory following and part sorting are presented. With jets, the UPM becomes a practical technology for applications such as part singulation, feeding, sorting, food handling, product displays, and interactive devices such as active desks and toys.*

1 Introduction

This paper is the culmination of our research on vibrations-based planar part manipulation. The work is centered on a device called the Universal Planar Manipulator (UPM), show in Figure 1. The UPM is a rigid horizontal plate actuated in its own plane (3 degrees of freedom) by external motors. As the plate vibrates rapidly, sliding friction causes parts such as coins, bottles, etc., to displace in a controlled manner.

The most interesting property of the UPM is its minimalism: despite its simple construction, the UPM can manipulate a large number of parts in parallel. Namely, given known locations of N parts, and N independent displacements desired for each part, a closed, rigid motion of the plate can be computed which, once executed, displaces all parts as desired. This result owes to the fact that, under Coulomb friction, distinct rigid rotations of the plate produce part displacement fields which are linearly-independent bases of the space of all possible part displacements [1, 2]. Namely, given desired displacements, a sum of (scaled) rigid plate rotations exists which produce them.

Figure 1: The Universal Planar Manipulator (UPM): generic objects placed on a flat plate can be manipulated independently via vibrations/friction.

One problem is that a rigid body cannot execute a motion in the space of summed rigid rotations. Fortunately, the sum space can be approximated by a sequence of $M \geq 2N$ rotations about known centers $\mathbf{C}_j$, $j = 1, 2, \cdots, M$, provided each rotation displaces parts by a small amount. This was exploited in our original method [1]: given part positions and desired displacements, the system solved for rotation durations k_j, a process which required inverting a matrix. Though linearly independent, rotations are not orthogonal: each rotation displaces all parts, resulting in a cross-talk matrix with much off-diagonal energy. The end result is that matrix inversion is ill-conditioned, so computed durations are long, and part displacements are slow and noisy. This was partly addressed by adding redundancy to the linear system, i.e., more rotations per parallel update, $M \gg 2N$. This slows down execution and does not rule out ill-conditioning.

The main contribution on this paper is to present a new motion primitive – called the *jet* – which diagonalizes the inversion process, so that the solving step is robust and execution is significantly sped up. A jet is a force field "focused" on a single part, which can be told do move while keeping all others still. Parallel manipulation then reduces to applying a jet to each part in sequence. Because the jet's action is local to a part, execution time is proportional to the number of parts being moved, irrespective of how many currently sit on the plate. In the previous method, N parts required at least $2N$ rotations, even if just a single part was being displaced.

The jet idea is supported by a complete characterization of the feeding forces produced when plate motion is a sum of two sinusoids. We derive specific conditions under which two sinusoids produce maximal or no feeding forces, based purely on their relative phase and frequency. With this theory, we are able to pick the components of plate motion which generate optimally-focused (as-local-as-possible) jets.

1.1 Related Work

The bowl feeder [3] is the canonical example of a vibrations-based manipulation device. Though stark in its simplicity, it is not a programmable device: its function is tied to part shape and its own internal track design. With the UPM, we attempt to preserve simplicity while allowing for programmable operation. Vibrations-based devices have been applied to sensorless manipulation: plate vibrations (non-rigid) produce force fields with local minima which automatically orient and/or localize various objects [4, 5]. This is impossible with the UPM since a force field produced by a rigid motion has zero divergence [1]. We use vision to provide the necessary sensory feedback. An active area of research has been *distributed manipulation*: is complex manipulation feasible with a large array of simple actuators? Many devices have been proposed, spanning both micro- and macro-scale applications, with or without sensors [2]. We have explored the complementary question of "how little is enough", the UPM being an extreme case: can a device with a single moving actuator be used to independently manipulate a large number of parts?

This paper is organized as follows: In Section 2 we describe the jet, our new local force field. In Section 3, the main parts of the UPM prototype are explained. Experiments using jet fields are presented in Section 4. In Section 5 we present a characterization of feeding forces with two harmonics. Conclusions are presented in Section 6.

2 The Jet as a Local Force Field

A new closed motion of S is described which integrates to a *local* force field called a jet. Local in the sense that it is only non-zero in the vicinity of a single part, and oriented along the part's desired motion.

Let the xy plane coincide with the horizontal plate S. S executes a *closed* motion lasting T seconds. "Closed" in the sense that at the end of the motion (time T) the surface returns to its initial position. Let $\mathbf{v}(\mathbf{P},t)$ denote the instantaneous velocity at a point $\mathbf{P}$ in S. Consider a part of mass m lying at point $\mathbf{P}$ on S. Assume the part's speed is negligible with respect to $\mathbf{v}(\mathbf{P},t)$. Assume plate motion is such that friction is always of the *sliding* type [6]. The part will perceive an instantaneous frictional force $\mathbf{f}(\mathbf{P},t)$ of fixed value μmg in the direction of $\mathbf{v}(\mathbf{P},t)$, where μ, g are the constant of sliding friction and the acceleration of gravity, respectively:

$$\mathbf{f}(\mathbf{P},t) = \mu mg \frac{\mathbf{v}(\mathbf{P},t)}{||\mathbf{v}(\mathbf{P},t)||} \tag{1}$$

Note: if $\mathbf{v} = \nu_x(t)$ is along a single direction, e.g., x, the above reduces to $\mu mg\,\mathrm{sgn}[\nu_x(t)]$. From Equation (1) obtain the frictional force $\bar{\mathbf{f}}$ applied to the part *averaged* over the entire motion:

$$\bar{\mathbf{f}}(\mathbf{P}) = \frac{\mu mg}{T}\int_0^T \frac{\mathbf{v}(\mathbf{P},t)}{||\mathbf{v}(\mathbf{P},t)||}dt \tag{2}$$

Consider a 1d translational vibration $\mathbf{v}(t)$ of S along $\mathbf{d} = (d_x, d_y)$, the *feeding direction*. $\bar{\mathbf{f}}$ will be non-zero if $\mathbf{v}(t)$ is *time-asymmetric*, i.e., its positive and negative (along $\mathbf{d}$) portions have different durations [7]. A $\mathbf{v}(t)$ with few sinusoidal components is desirable since it avoids resonances in the mechanical system. Non-zero $\bar{\mathbf{f}}$ requires at least two sinusoids, since a single sine is time-symmetric. Corollary 1 in Section 5 states that the velocity profile:

$$\mathbf{v}(t) = \mathbf{d}[\cos(t) - \cos(2t)] \tag{3}$$

delivers the maximum possible force $\mu mg/3$ in the feeding direction over all choices of frequencies and phases for two sinusoids. To the above 1d motion, consider superimposing a sinusoidal rotation about a point $\mathbf{C}$, namely:

$$\mathbf{v}(\mathbf{P},t) = \mathbf{d}[\cos(t) - \cos(2t)] + \frac{2|\mathbf{d}|}{\rho}\sin\left(\frac{2}{3}t\right)(\mathbf{P}-\mathbf{C})^{\perp} \tag{4}$$

Where ρ is a scaling constant for the rotation component. This motion is closed with period $T = 6\pi$. Near $\mathbf{C}$ the rotation component vanishes, and Equation (4) reduces to Equation (3). At large radii from $\mathbf{C}$, the rotation component (i.e., tangential velocities) dominates. Since this signal is time-symmetric, it will produce zero feeding forces. At distance ρ from $\mathbf{C}$, the rotational and translational waveforms have equal peak values. So parameter ρ can be set to control the rate of decay from maximum feeding force at $\mathbf{C}$ to zero at infinity. The larger the ρ, the more the field's active zone is "focused" (i.e., concentrated) on $\mathbf{C}$.

We chose $\sin(2t/3)$ for the rotational component so as to produce zero feeding forces with either component of Equation (3). This helps in creating "destructive interference" (in the feeding force sense) anywhere but in the vicinity of $\mathbf{C}$. We now refer to the results derived in Section 5. First, $\sin(2t/3)$ is non-feeding with $\cos(2t)$ because their frequencies are at a 1:3 ratio. Because both these numbers are odd, $\bar{\mathbf{f}} = 0$, Lemma 1. Second, $\sin(2t/3)$ is non-feeding with $\cos(t)$ because though their frequencies are at a 2:3 ratio (this is potentially feeding, Lemma 3), their phases are such that both waveforms have at least one coinciding root (at $t = 3\pi/2$), so $\bar{\mathbf{f}} = 0$, Corollary 2.

Other possible choices for the rotation component are $\sin(t) + \cos(t)$, $\sin(2t)$, and so on to higher frequencies. We opted for going below the feeding fundamental since for a given motor power, higher peak rotational velocities ($\propto \rho$) are feasible, yielding better-focused fields.

By plugging Equation (4) into the average force field integral, Equation (2), we obtain an average force field which is "local" to $\mathbf{C}$, as shown in Figure 2. We call this primitive a "jet", since it resembles a field of the same name in fluid mechanics. Under a jet field, only a part at $\mathbf{C}$ will experience any feeding force at all.

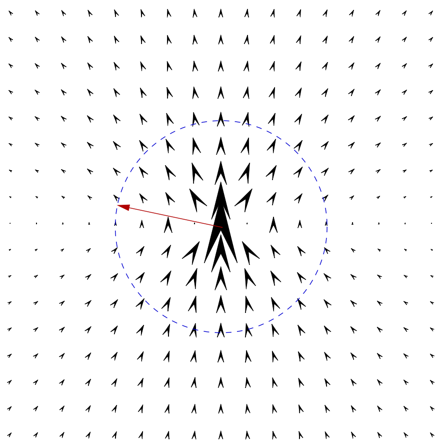

Figure 2: The jet force field: a feeding velocity $\hat{y}[\cos(t) - cos(2t)]$ superimposed to a rotation $\sin(2t/3)/\rho$ about the origin. Frictional forces are represented by scaled arrows. The dotted circle – a measure of the jet's focus – has radius 2ρ.

A straightforward step is to compute controls (forces and torques) which will position and orient the jet at will. Parallel manipulation then reduces to applying jets to individual parts, in round-robin fashion: for each part (i) track coin positions $\mathbf{P}_i, i = 1, 2, \cdots, N$ using vision; (ii) get desired displacements $\mathbf{d}_i$ from task; (iii) apply a jet field focused on $\mathbf{P}_i$ and oriented along $\mathbf{d}_i$.

Because local fields are nearly orthogonal (little cross talk), the solving step is direct (no matrix inversion required). While parts away from the jet's center do flow a bit (the field is small but non-zero there), this can be easily corrected with vision feedback. Jet-based manipulation is also much more scalable: if a subgroup of N_0 parts needs to be manipulated within a group of N parts only $N_0 \leq N$ jets are needed. In the old method, this required at least $2N$ rotations [1].

3 UPM Details

A block diagram of our prototype appears in Figure 3. Its various parts are explained next.

The plate itself is a 16"x16" tile of honeycomb material. Honeycomb is both cheap and has a very large stiffness-by-density ratio [8], i.e., vertical oscillations of the plate are kept to a minimum. The plate is constrained to move in its own plane by four vertical nylon rods supporting each of the plate's corners. This bearingless, flexure system is ideal since plate oscillations are of just a few millimeters.

Four voice coils (delivering up to 50 lbf each) actuate the plate in two differential pairs, along x and y. Each can apply either a force or a torque to the plate, depending on whether input signals are in- or out-of-phase, respectively.

For calibration purposes, two 2-axis accelerometers are installed at opposite corners of the plate. Prior to an experiment, the plate is run through a battery of standard motions; accelerometer data is used to compensate for distortions.

A camera is mounted over the plate and feeds color NTSC back to the controlling PC. This is used to locate the table's edges and track moving parts ("visual" feedback).

An interface board containing two micro-controller chips manages both the sampling of accelerometer signals and the generation of four phase-precise analog signals to the motors. A consumer-grade audio amplifier boosts the four analog signals to power levels required by each motor. To synthesize a jet, the PC downloads appropriate waveform parameters to the interface board. The PC commands the the board to issue a pulse (a few cycles) of the four analog waveforms, causing the plate to vibrate and the parts to displace. Parts' positions are re-tracked, and the process repeats.

The jet waveform, Equation (4), injects three frequencies into the plate, call them f, $2f$, and $2f/3$. We found that $f = 35$Hz avoided any natural resonances of the system, while allowing for large peak velocities with the existing motors (large peak velocities promote both strong feeding forces and good jet focusing).

4 Experiments

Parallel manipulation under the new method is demonstrated in two experiments. First, we attempt to move three pennies along the same bowtie curve, Figure 4. In this 6-dof system, pennies have to reorganize themselves in a clearly non-rigid way as they traverse the curve. The controller ensures pennies remain equidistant from each other

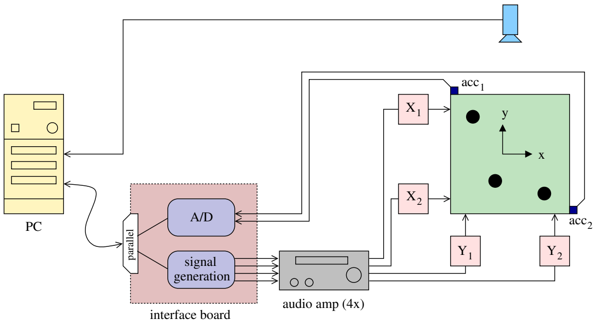

Figure 3: Block diagram of the UPM. Three parts (dark disks) are shown on the surface of the plate. The plate is actuated by four external voice coils (linear motors), organized in pairs X_1X_2 and Y_1Y_2. Two 2-axis accelerometers acc_1 and acc_2 are installed at opposite corners of the plate. A PC is connected to an interface board via a parallel port. The PC passes to the board motion parameters (phases, amplitudes, frequencies) for four independent analog signals. The board generates four signals with phase-precision. The signals are amplified by an audio amplifier and then fed to the four motors. The accelerometer signals (four in total) are sampled at the interface board and passed back to the PC for calibration purposes.

as they move along the curve. For each update of the three coins, the system applies three jets, each centered at a specific coin. To speed up execution, a jet is executed in parallel with part tracking and motion computation for the next part (jet execution is the bottleneck). Snapshots of the experiment are shown in Figure 5

A second experiment involves the sorting of 8 plastic poker chips (a 16-dof system) based on color, Figure 6. Light and dark chips need to go to opposite sides of the UPM. An automatic labelling of part color is done by the vision system. The control loops involves applying jets to each individual part in the appropriate direction, round-robin. A better approach would include motion planning (e.g., using potential fields) but here the controller simply pushes chips to the appropriate side. Videos of these experiments can be found on the web at: `www.cs.berkeley.edu/~dreznik/UPM2000/`

Manipulation with the UPM is not restricted to disk-shaped objects. As shown in Figure 1, this device can manipulate generic objects such as tools, bottles, etc. Because force scales with weight, objects with different weights will move at similar speeds, provided they have similar friction coefficients with the plate.

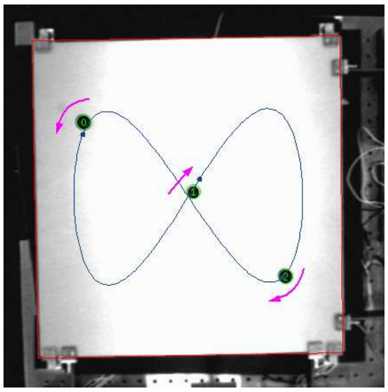

Figure 4: Bowtie experiment as viewed from the overhead camera. Three pennies and the intended bowtie curve are shown.

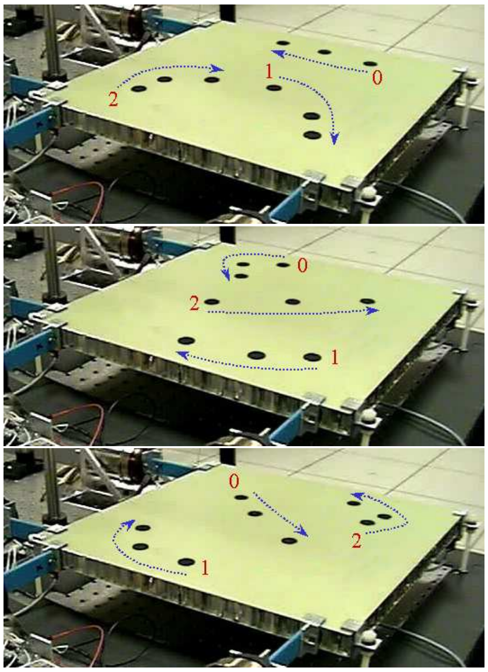

Figure 5: Snapshots of motion along the bowtie curve. Each snapshot combines 3 consecutive frames in "stop motion". Arrows label part motion across frames. Parts complete a loop around the bowtie in about a minute.

5 Part Feeding with two Sinusoids

In this Section, we characterize the frictional forces produced by plate motion made up to two sinusoids. The less mathematically inclined should skip the details and simply review the lemmas, theorem, and corollaries.

Consider a flat horizontal surface S; let the xy-plane lie on its surface, with the z-axis pointing upwards, opposite to gravity. Consider a rigid vibration of S along x, with

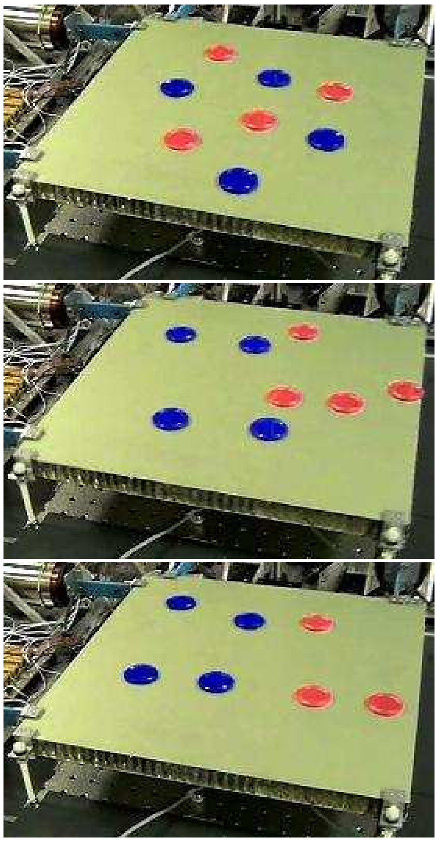

Figure 6: The sorting experiment: eight plastic poker chips (4 dark/blue, and 4 light/red) initially scattered randomly over the device (top) are sorted by color to opposite sides of the plate. In the last frame, one of the light chips has fallen the right edge of the table. All chips get sorted in about 30 seconds.

velocity $\nu(t)$ of the form:

$$\nu(t) = \sin(f_1 t) + b \sin[f_2(t - \varphi)] \tag{5}$$

Parameters b and φ are relative amplitude and phase between the components. t and φ are given in radians. We consider the case of f_2/f_1 rational, $f_2 \geq f_1$. Let n_2/n_1 be the reduced fractional representation of f_2/f_1 in terms of two relatively prime integers [9] n_2, n_1, with $n_2 \geq n_1$, $\gcd(n_1, n_2) = 1$. Without loss of generality, we normalize $\nu(t)$'s period to 2π by writing:

$$\nu(t) = \sin(n_1 t) + b \sin[n_2(t - \varphi)] \tag{6}$$

Consider a part P lying on S with negligible velocity $\nu_p(t) \cong 0$, i.e., S's velocity relative to P is simply $\nu(t)$. We use Coulomb friction in sliding mode [6] as our model: the force S applied to P is (i) in the direction of $\nu(t)$, and (ii) of constant magnitude $\mu m g$, where μ, m, g symbolize the frictional constant, the part's mass, and the acceleration of gravity, respectively. Then the average frictional force $\bar{f}$ applied to P per cycle is:

$$\bar{f} = \frac{\mu m g}{2\pi} \int_0^{2\pi} \mathrm{sgn}[\nu(t)] dt \tag{7}$$

where $\mathrm{sgn}[u]$ is the sign function, defined as $1, u \geq 0$, and -1 otherwise.

Lemma 1. *If both n_1 and n_2 are odd then $\bar{f} = 0$, for any choice of b, φ.*

Proof. A sinewave has the symmetry $\sin(nt) = -\sin[n(t - \pi)]$, $\forall t$, provided n is odd. When both n_1 and n_2 are odd, each of Equation (6)'s harmonics will display this type of symmetry, and thus $\nu(t) = -\nu(t - \pi)$, i.e., $\mathrm{sgn}[\nu(t)]$ integrates to zero in $[0, 2\pi)$. □

Lemma 2. *For any choice of n_1, n_2, b, a phase φ exists which causes $\bar{f} = 0$, for any b.*

Proof. Choose $\varphi = 0$: $\nu(t)$ is a sum of two pure sines, i.e., it is an odd function with symmetry $\nu(t) = -\nu(-t)$. So Equation (7) integrates to zero. □

Lemma 3. *If one of n_1, n_2 is even[1] then $\bar{f} \neq 0$ for some b, φ.*

Proof. First we choose a phase which gives feeding, namely we adjust φ so that the positive peak of the n_1 sinusoid aligns with the negative peak of n_2, allowing $\nu(t)$ to be written from Equation (6) as:

$$\nu(t) = \cos(n_1 t) - b \cos(n_2 t) \tag{8}$$

Now rewrite Equation (8) as the following product (using standard trig identities):

$$\nu(t) = 2 \sin\left(\frac{\alpha t}{2}\right) \sin\left(\frac{\beta t}{2}\right) \tag{9}$$

where $\alpha = n_2 - n_1$ and $\beta = n_2 + n_1$. Because exactly one of n_1, n_2 is even, both α, β are odd. It is also true that α, β are relatively prime since $\gcd(\alpha, \beta) = \gcd(\alpha - \beta, \beta) = \gcd(2n_2, \beta) = \gcd(\alpha, 2n_1)$. Therefore $\gcd(\alpha, \beta)$ is also a divisor of $2n_2$ and $2n_1$ and therefore of $2\gcd(n_1, n_2) = 2$. But it can't be two since α and β are odd. Thus $\gcd(\alpha, \beta) = 1$.

Since α and β are relatively prime, their least common multiple – the *lcm* – is given by their product:

$$\mathrm{lcm}(\alpha, \beta) = \alpha\beta = n_2^2 - n_1^2 \tag{10}$$

[1] They can't both be even since they're relatively prime.

$\nu(t)$ has a root whenever either of Equation 9's factors is zero, i.e., t is a multiple of either $2\pi/\alpha$ or $2\pi/\beta$. Equivalently, the roots of $\nu(t)$ may only occur at "grid points" $t_k = 2k\pi/(\alpha\beta)$, $k = 0, 1, \cdots, \alpha\beta$. Define open intervals $\sigma_k = (t_{k-1}, t_k)$, $k = 1, 2, \cdots, \alpha\beta$, each of equal length $2\pi/(\alpha\beta)$. Within each σ_k, $\nu(t)$ has no roots, i.e., it is of constant sign. So the integral in Equation (7) becomes the following discrete sum:

$$\bar{f} = \frac{\mu m g}{\alpha\beta} \sum_{k=1}^{\alpha\beta} \operatorname{sgn}[\nu(\sigma_k)] \tag{11}$$

We note the quantity $\alpha\beta$ is odd, since it is the product of two odd numbers, i.e., Equation (11) is a sum of an odd number of ± 1's. An imbalance must exist in this sum, and therefore $\bar{f} \neq 0$. $\square$

Because $\bar{f}$ is a continuous function of b, φ, property $\bar{f} \neq 0$ holds true within an open neighborhood of $b = 1$ and the φ chosen to render $\nu(t)$ of the form of Equation (8).

The previous result is illustrated in Figure 7 for the case where $n_1 = 2$ and $n_2 = 5$. The sign imbalance in this example is exactly one σ_k, which turns out to be the maximum possible imbalance, explained next.

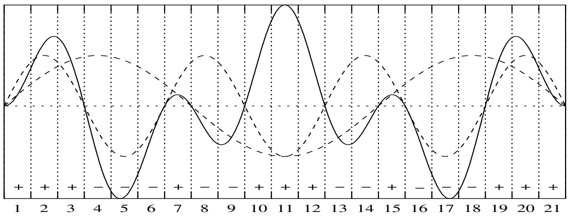

Figure 7: Sign imbalance for the case $n_1 = 2$ and $n_2 = 5$, i.e., $\alpha = 3$, $\beta = 7$. $\nu(t) = cos(2t) - cos(5t)$ is plotted as a solid curve over the $[0, 2\pi)$ interval. Its two factors: $sin(\frac{3}{2}t)$, and $sin(\frac{7}{2}t)$, are plotted as dashed curves. $\operatorname{lcm}(\alpha, \beta) = \alpha\beta = 21$ yields the number of equal-length sub-intervals of $[0, 2\pi]$ which preserve the sign of $\nu(t)$; in the above, intervals are numbered and identified with a "+" or "-", according to ν's sign in that interval. Because $\alpha\beta$ is odd, the number of positive- and negative-sign intervals must differ: above one counts 11 positive vs. 10 negative intervals. This implies $\bar{f} \neq 0$.

Theorem 1. *Consider a surface velocity of the form:*

$$\nu(t) = \cos(n_1 t) - \cos[n_2(t - \psi)] \tag{12}$$

where $n_2 > n_1$ are relatively prime, and exactly one is even. $\psi = 0$ yields the maximum possible average force $\bar{f} = \mu m g/(n_2^2 - n_1^2)$. In general, $\bar{f}$ is a triangular waveform on ψ, taking the following form:

$$\bar{f} = \frac{\mu m g}{n_2^2 - n_1^2} \triangle(n_1 n_2 \psi) \tag{13}$$

where $\triangle(t)$ is a unit-amplitude, triangular waveform of period 2π:

$$\triangle(t) = \begin{cases} 1 - 2|t|/\pi, & |t| < \pi \\ \triangle(|t| - 2\pi), & \textit{otherwise} \end{cases}$$

Proof. First, using trigonometric product formulae, rewrite Equation (12) as the product:

$$\nu(t) = \sin\left[\frac{\alpha}{2}(t - \psi_1)\right] \sin\left[\frac{\beta}{2}(t - \psi_2)\right] \tag{14}$$

$$\psi_1 = \frac{n_2}{n_2 - n_1}\psi \tag{15}$$

$$\psi_2 = \frac{n_2}{n_2 + n_1}\psi \tag{16}$$

where α, β are defined as in Equation (9). With the substitution $t \to t - \psi_1$ obtain:

$$\nu_\Psi(t) = 2h_\alpha(t)h_\beta(t - \Psi) \tag{17}$$

where $h_n(t)$ stands for $\sin(nt/2)$, and $\Psi = \psi_2 - \psi_1$ is obtained from Equations (15) and (16):

$$\Psi = \frac{-2n_1 n_2}{n_2^2 - n_1^2}\psi \tag{18}$$

Equation (17) has roots when either factor is zero, i.e., t is a multiple of either $2\pi/\alpha$ or $2\pi/\beta$. Let a time t for which both factors vanish be called a *common root*.

Case 1. $\Psi = 0$

By inspection, $t = 0$ is a common root, and no others may exist in $[0, 2\pi)$, as this would imply two non-negative integers $k_1 < \alpha$ and $k_2 < \beta$ exist such that $2\pi k_1/\alpha = 2\pi k_2/\beta$, i.e., $k_1\beta = k_2\alpha$. Because $\gcd(\alpha, \beta) = 1$, this is impossible. Notice that $\Psi = 0$ implies $\psi = 0$, Equation (18). Lemma 3 tells us that for $\psi = 0$, $\bar{f} \neq 0$. Call this non-zero average force $\bar{f}_0$. In general, we will use $\bar{f}_\Psi$ to denote the average force for the phase Ψ defined above.

Case 2. $0 < \Psi < \frac{2\pi}{\alpha\beta}$

In this range there are no common roots since none of $h_\beta(t - \Psi)$'s roots fall on integral multiples of $2\pi/(\alpha\beta)$. Let $r_k = 2k\pi/\beta$ denote the kth root of $h_\beta(t)$. Define β intervals η_k:

$$\eta_k = (r_k, r_k + \Psi) \; k = 0, 1, \cdots \beta - 1$$

The η_k represent the "sweep" of the zeros of h_β as Ψ varies. Notice that for t in one of the η_k, the signs of the shifted waveform $\nu_\Psi(t)$ and the unshifted $\nu(t)$ will be different, while they will be the same for t outside those intervals.

By a slight abuse of notation, let $\operatorname{sgn}(\eta_k)$ denote the sign of $\nu_\Psi(t)$ in the interval η_k. Since $\nu(t)$ and $\nu_\Psi(t)$ differ exactly in the η_k, the net feeding force will be changed by exactly their contributions. In other words, from equation (7), we get that:

Remark 1. *The change in feeding force is the sum of changes due to the intervals η_k, or:*

$$\bar{f}_\Psi = \bar{f}_0 + \frac{\mu m g}{2\pi} 2\Psi \sum_{k=0}^{\beta-1} \operatorname{sgn}(\eta_k)$$

where Ψ is included because it is the length of every interval η_k, and thus equal to the magnitude of the integral of the sign function over the η_k; and 2 is included because each interval of length Ψ contributes by its own sign, but also by reducing the integral of regions of the opposite sign.

We complete the proof by showing that only η_0 contributes to the sum. The rest cancel each other in symmetric pairs.

Now $h_\alpha(t)$ is symmetric in the interval $[0, 2\pi]$, i.e., $h_\alpha(t) = h_\alpha(2\pi - t)$, and in particular, $h_\alpha(r_k) = h_\alpha(r_{\beta-k})$. Furthermore, because $h_\alpha(t)$ has no roots within the η_k's, we can infer:

$$\operatorname{sgn}[h_\alpha(\eta_k)] = \operatorname{sgn}[h_\alpha(\eta_{\beta-k})],\ \forall k > 0 \qquad (19)$$

$h_\beta(t)$ is also symmetric in $[0, 2\pi]$, but more importantly, its derivative is anti-symmetric. That is, $h'_\beta(t) = -h'_\beta(2\pi - t)$. This implies that $h_\beta(t)$'s zero-crossings at r_k and $r_{\beta-k}$ are in opposite directions, and thus:

$$\operatorname{sgn}[h_\beta(\eta_k)] = -\operatorname{sgn}[h_\beta(\eta_{\beta-k})], \forall k > 0 \qquad (20)$$

Since $\operatorname{sgn}(\eta_k) = \operatorname{sgn}[h_\alpha(\eta_k)] \operatorname{sgn}[h_\beta(\eta_k)]$, the last two equations tell us that

$$\operatorname{sgn}[\eta_k] = -\operatorname{sgn}[\eta_{\beta-k}], \forall k > 0 \qquad (21)$$

For β ranging from $0, \ldots, \beta - 1$, this means that only η_0 is missing a partner of opposite sign. All the other terms cancel and we have shown that only η_0 contributes to the sum in remark 1. Since $\operatorname{sgn}[\eta_0] = -1$, remark 1 simplifies to:

Remark 2. *The change in feeding force with Ψ is due entirely to η_0, and is equal to:*

$$\bar{f}_\Psi = \bar{f}_0 - \frac{\mu m g}{\pi} \Psi \qquad (22)$$

These concepts are illustrated in figure 8.

Case 3. $\Psi = 2\pi/(\alpha\beta)$

Remark 3. *At $\Psi = 2\pi/(\alpha\beta)$ a new common root $t_k = 2k\pi/\alpha\beta$ is generated at some k, which is unique in the range $t \in [0, 2\pi]$.*

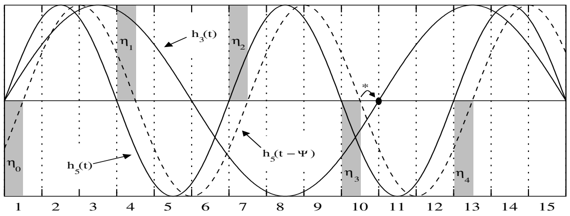

Figure 8: Force cancellation for $\alpha = 3$, and $\beta = 5$ (15 constant-sign intervals). The two solid curves are $h_3(t) = \sin(3t/2)$ and $h_5(t) = \sin(5t/2)$. The dashed curve is $h_5(t - \Psi)$, where Ψ is $\pi/(\alpha\beta)$, i.e., half a basic interval. The η_k intervals appear shaded above (resp. below) the x-axis depending on the sign of $h_\alpha(t)h_\beta(t - \Psi)$. Each η_k cancels with $\eta_{\beta-k}$, with the exception of η_0; so the canceling pairs are (η_1, η_4), (η_2, η_3). As Ψ approaches a full interval's length, a new common root is generated at the end of the 10th interval, marked with a "*".

To show this let $t' = t\alpha\beta/(2\pi)$. So $\nu(t')$ has period $\alpha\beta$ and the roots of $h_\alpha(t')$ [resp. $h_\beta(t')$] are on integers $t = k_1\beta,\ k_1 = 0, 1, \cdots, \alpha$ [resp. $t = k_2\alpha,\ k_2 = 0, 1, \cdots, \beta$]. Conveniently, $h_\beta(t - 2\pi/\alpha\beta)$ becomes $h_\beta(t' - 1)$, so we need to show that $h_\alpha(t')$ has a root exactly one unit above a root of $h_\beta(t')$, i.e., a unique pair k_1, k_2 exists such that $k_1\beta = k_2\alpha + 1$.

Because α and β are co-prime, this is exactly Bézout's relation [9], which guarantees that a unique solution pair (k_1, k_2) exists modulo $\alpha\beta$. For example, if $\alpha = 3$, $\beta = 5$, $k_1 = 2$ and $k_2 = 3$ is the unique solution, i.e., the common root corresponding to a unit shift occurs at $t' = k_1\beta = 10$, Figure 8.

Remark 4. *At $\Psi = 2\pi/(\alpha\beta)$, $\nu_\Psi(t)$ is identical to $\nu(t)$ up to a sign flip and a shift by the common root t_k, i.e.:*

$$\nu_{(2\pi/\alpha\beta)}(t) = \pm\nu(t - t_k)$$

This is true because the factors $h_\alpha(t)$ and $h_\beta(t - 2\pi/\alpha\beta)$ are sinusoids. When shifted by a multiple of their root separation, sinusoids are identical up to a sign change. When a product of two sinusoids is shifted by a common root, the resulting function is also identical up to a sign change.

Equation (22) tells us that at $\Psi = 2\pi/\alpha\beta$, $\bar{f}_\Psi = \bar{f}_0 - 2\mu m g/\alpha\beta$, a non-zero change. Remark 4 tells us that $\nu_\Psi(t) = \pm\nu(t - t_k)$ and therefore $\bar{f}_\Psi = \pm\bar{f}_0$. But since there is a finite change, we cannot have $\bar{f}_\Psi = \bar{f}_0$, so we must have $\bar{f}_\Psi = -\bar{f}_0$. Their difference is $2\mu m g/\alpha\beta$, and so

$$\bar{f}_0 = \frac{\mu m g}{\alpha\beta} = \frac{\mu m g}{n_2^2 - n_1^2} \qquad (23)$$

We can re-apply this argument to the next interval of $\Psi \in [2\pi/(\alpha\beta), 4\pi/(\alpha\beta)]$ and we would see a change in $\bar{f}$ in the opposite direction back to the original $\bar{f}_0$. Within each interval, $\bar{f}_\Psi$ varies linearly with Ψ, and so it generates a triangular waveform.

From Equation (18) we see that $\Psi = 2\pi/(\alpha\beta) = 2\pi/(n_2^2 - n_1^2)$ corresponds to $\varphi = -\pi/(n_1 n_2)$. Therefore, for $\varphi \in (0, 2\pi)$, $\bar{f}(\varphi)$ will hit $\pm\bar{f}_0$ $2n_1n_2$ times. Because the change in $\bar{f}$ is linear on Ψ, φ, Equation (22), and because the peaks alternate, $\bar{f}(\varphi)$ must also be a triangular waveform whose period is 2π divided by half the number of peaks, i.e., its period is $2\pi/(n_1 n_2)$, and of amplitude given by the peak value, Equation (23). $\square$

The shape of $\bar{f}$ as a function of φ for various n_1, n_2 combinations is illustrated in Figure 9.

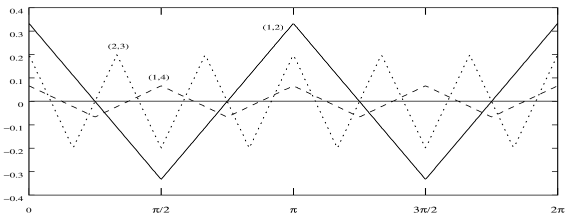

Figure 9: Plot of $\bar{f}/(\mu m g)$ versus ψ for $(n_1, n_2) = \{(1,2), (2,3), (1,4)\}$. The points plotted were obtained through numeric integration. As predicted, the function is a triangular waveform of period $2\pi/(n_1 n_2)$ and of amplitude $1/(n_2^2 - n_1^2)$.

Corollary 1. *The choice* $n_1 = 1$, $n_2 = 2$, *and* $\psi = 0$ *yields the highest possible* $\bar{f} = \mu m g/3$.

Proof. At $\psi = 0$, the triangular waveform is at a peak. We know $n_2 \geq n_1 + 1$. Therefore the denominator of $\bar{f}$ is:

$$n_2^2 - n_1^2 \geq (n_1 + 1)^2 - n_1^2 = 2n_1 + 1$$

And this bound is attained (i.e., $\bar{f}$ is maximized) when $n_2 = n_1 + 1$; the global minimum of this expression (and the global maximum of $\bar{f}$) occurs when $n_1 = 1$ and $n_2 = 2$, yielding $\bar{f} = \mu m g/3$. $\square$

In practice, we typically use $\nu(t) = \cos(t) - \cos(2t)/2$ ($b = 1/2$); though this yields $\bar{f} \cong 0.24\mu m g$ (lower than the $b = 1$ case) it also yields a higher equilibrium velocity.[2]

Corollary 2. *A sum of harmonics* n_1, n_2 *(exactly one of which is odd) produces zero (resp. maximum) feeding force if they have at least one root (resp. peak) aligned.*

Proof. When at least one root (resp. peak) is aligned, the sum waveform is equivalent (modulo a phase shift and a sign flip) to a sum of pure sines (resp. cosines), which yields zero (resp. maximum) feeding force, Lemma 2 (resp. Theorem 1). $\square$

[2] The part's equilibrium velocity ν_p is such that $\mathrm{sgn}[\nu(t) - \nu_p]$ integrates to zero in 2π.

6 Conclusion

A new local motion primitive called the "jet" has been described which makes parallel manipulation with the UPM fast and robust, overcoming many of the shortcomings present in a previous method. Optimum jet components were chosen based on a complete characterization of feeding forces when plate motion is a sum of two sinusoids. Due to its mechanical simplicity, the UPM is an attractive technology for existing industrial applications such as part feeding, sorting, singulation, etc. The "open face" nature of its workspace suggests interesting applications in novel areas such as product display, interactive toys, and active desks. Future work with the UPM includes manipulation of generic objects such as tools, and bottles. This will require both more sophisticated vision software and the ability to rotate parts, e.g., by applying localized force couples.

References

[1] D. Reznik and J. Canny. A flat rigid plate is a universal planar manipulator. In *IEEE International Conference on Robotics and Automation*, Leuven, Belgium, May 1998.

[2] K. Bohringer and H. Choset. *Distributed Manipulation*. Kluwer Academic Publishers, Norwell, MA, 2000.

[3] G. Boothroyd. *Assembly automation and product design*. Marcel Dekker, Inc., New York, NY, 1991.

[4] V. Hayward, N. Tran, and K. Chan. Object behavior using a vibrating plate testbed for part presentation research. EE304-494 project writeup, McGill University, December 1995.

[5] K. Böhringer, V. Bhatt, and K. Goldberg. Sensorless manipulation using transverse vibrations of a plate. In *IEEE International Conference on Robotics and Automation*, Nagoya, Japan, May 1995.

[6] R. Resnick and D. Halliday. *Physics, part I*. John Wiley & Sons, Inc., New York, NY, 11th edition, 1987.

[7] D. Reznik and J. Canny. The coulomb pump: A novel parts feeding method using a horizontally-vibrating surface. In *IEEE International Conference on Robotics and Automation*, Leuven, Belgium, May 1998.

[8] L. Gibson and M. Ashby. *Cellular Solids: Structure and Properties*. Cambridge University Press, Cambridge, MA, 1999.

[9] M. Mignotte. *Mathematics for Computer Algebra*. Springer-Verlag, New York, NY, 1992.